ChemComm

COMMUNICATION

Teaching photosensitizers a new trick: red light-triggered G-quadruplex alkylation by ligand co-localization†

Enrico Cadoni, [a] Alex Manicardi, [a] Mathieu Fosséprè, [b] Kaat Heirwegh, [a] Mathieu Surin *[b] and Annemieke Madder *[a]

Cite this: *Chem. Commun.*, 2021, **57**, 1010

Received 10th September 2020, Accepted 1st December 2020

DOI: 10.1039/d0cc06030e

rsc.li/chemcomm

We propose a bimolecular approach for G-quadruplex alkylation, using a pro-reactive furan-containing ligand, activated by red-light irradiation of a proximate G4-binding photosensitizer. G4- over dsDNA alkylation can be achieved selectively and proves high-yielding at low ligand excess. HPLC and modelling studies allowed identifying potential residues involved in the alkylation.

G-Quadruplexes (G4s) are well-known structures that can be formed in the promoter region of numerous and relevant proto-oncogenes as well as in human telomeric regions.[1] Recent evidence that such structures could be formed *in vivo* under physiological conditions justifies the efforts directed towards the design of molecules capable of stabilizing G4s in a selective manner.[2] While most of the available ligands engage in non-covalent interactions with G4-DNAs, also examples of G4-alkylating agents exist.[3] However, most of them rely on highly reactive moieties which can show off-target reactions, compromising their G4-selectivity. Alternative and elegant approaches involve the use of pro-reactive moieties which can be activated by external stimuli, allowing spatiotemporal control, reducing collateral damage and preventing premature degradation of the ligands. In therapeutic contexts light is a practical stimulus, but photo-alkylation procedures are poorly explored and often require harmful UV-irradiation that may limit their applicability.[4] Our group has previously reported on furan-based methodologies for DNA–DNA and PNA–DNA interstrand crosslinking.[5] Pro-reactive furan can be oxidized into a reactive keto–enol, which rapidly reacts with exocyclic amines of DNA nucleobases. The activation can be conveniently triggered by singlet oxygen ($^1O_2$), generated *in situ* by light irradiation of a photosensitizer (PS).[6] In this study, we apply this methodology to a small molecule–DNA interaction, using furan-modified G4 ligands to covalently target G4 structures (Fig. 1).

To achieve this goal, we synthesized a previously reported furan-containing ligand (**TAP-A**). G4 c-Kit, a reported target for **TAP-A**, was used as a model sequence for the optimization.[7] We first evaluated which PS suited best for furan activation, reasoning that employing a G4-binding PS, such as methylene blue (MB),[8] could guarantee local $^1O_2$ generation, thus reducing collateral oxidative damage. At the same time, the high tissue penetration of the red-light wavelengths needed for $^1O_2$ production (660 nm) makes its use more suitable for therapeutic applications.[9] When comparing $^1O_2$ generation by MB *versus* Rose Bengal (RB, a PS with similar quantum yield[10] but not able to bind G4, see ESI,† Section 3 for further discussion) through monitoring of ABDA degradation, a decreased ABDA quenching by MB in presence of G4-DNA was noted (Fig. S4 and Table S1, ESI†), while a faster **TAP-A** oxidation was observed in the combined presence of MB and G4-DNA (Fig. 2). In contrast,

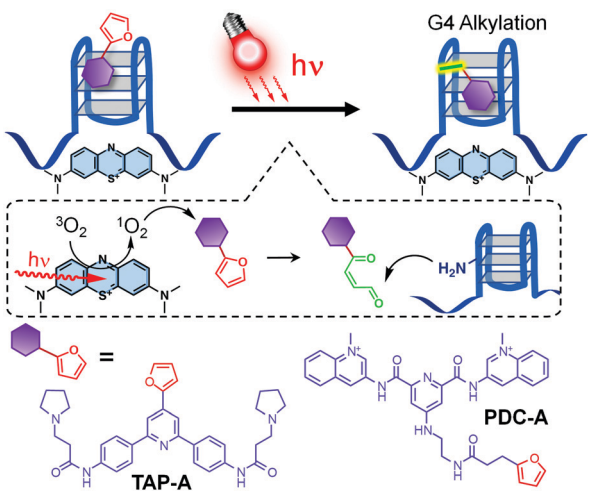

Fig. 1 Proposed furan-based light-triggered G4-DNA alkylation.

[a] *Organic and Biomimetic Research Group, Faculty of Sciences, University of Ghent Campus Sterre, Krijgslaan 281, Building S4, B-9000 Gent, Belgium. E-mail: annemieke.madder@ugent.be*

[b] *Laboratory for Chemistry of Novel Materials, Center of Innovation and Research in Materials and Polymers, University of Mons, Place du Parc 20, B-7000 Mons, Belgium. E-mail: mathieu.surin@umons.ac.be*

† Electronic supplementary information (ESI) available. See DOI: 10.1039/d0cc06030e

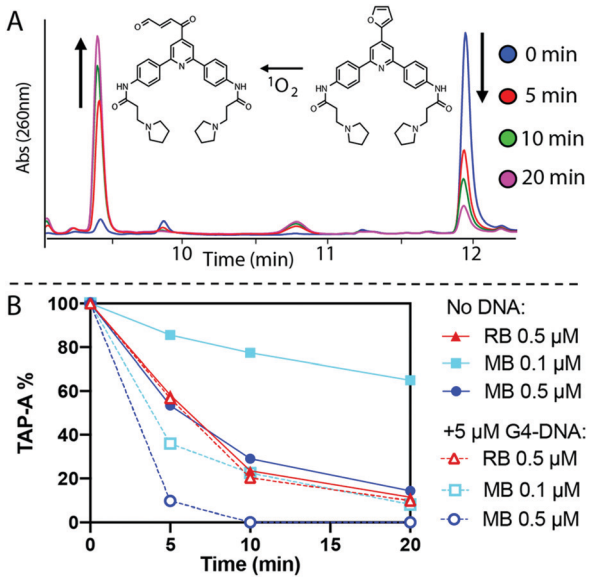

Fig. 2 **TAP-A** oxidation studies. (A) Activation mechanism and HPLC-UV traces of a typical experiment; (B) Ligand consumption profile (25 μM), using PSs in absence (continuous) or presence (dashed) of G4-DNA. Experiment performed in Tris HCl buffer (pH 7.4, 10 mM K^+) at 25 °C.

the ability of RB to quench ABDA was not influenced by the presence of G4-DNA. This indirectly indicates the co-localization of both ligand and PS on the G4-DNA in the case of MB, thus allowing a general reduction of $^1O_2$ levels while maintaining efficient furan oxidation. This effect is even more pronounced at low (0.1 μM) PS concentration.

Next, the alkylation efficiency of **TAP-A** in presence of the target G4-sequence was evaluated in buffered solutions (pH 7.4, 10 mM KCl), using a 5-fold excess of ligand with respect to the target to ensure formation of the G4-ligand complex, as previously reported.[7] MB concentration was kept at 0.1 μM. The mixtures were irradiated for 30 min and analysed by HPLC-UV. Both DNA and ligand signals decreased upon light irradiation, leading to the formation of new peaks (Fig. 3), which were purified and analysed *via* MALDI-TOF (Fig. 3, insert). Mass analysis revealed the formation of two alkylation products: while the first, single peak (rt = 7.9 min) showed the presence of the mono-alkylation adduct, the two close signals (rt = 8.2 min) revealed the presence of mono and di-alkylation products (+576 Da and +1152 Da, respectively). Based on HPLC-chromatogram integration, up to 73.5% of c-Kit reacted and was, as can be reasonably assumed, converted to an alkylated product, as no significant DNA oxidation was observed in absence of ligand (Fig. S7, ESI†). Additionally, in presence of alternative DNA structures (mutated c-Kit ssDNA and dsDNAs, see Fig. 3A) no significant differences were found in the DNA HPLC profiles after irradiation (see ESI,† Fig. S12), thus confirming the high G4-selectivity of this methodology. Moreover, even at 2.0 μM PS concentration, which ensures complete oxidation of the ligand (Fig. 3C), no alkylation of non-G4-DNAs was observed. The G4-selectivity over dsDNA was further confirmed by competition experiments, were increasing amounts of dsLAC were added to a c-Kit solution (please see ESI,† Section 8).

To identify the residues involved in the alkylation, we decided to systematically substitute the bases in the loops with unreactive thymines (G4-forming ability was confirmed by UV-melting experiments at 295 nm, Table S3, ESI†).[11] Substitution of C1 (Fig. 4, C1 → T), led to the disappearance of the di-alkylation peaks (rt = 8.2 min), while retaining the single signal corresponding to mono-alkylation product (rt = 7.9 min). Interestingly, when substituting all the reactive residues (LT in Fig. 4), a similar alkylation profile was maintained. This is a clear indication that alkylation occurs on C1 as well as on a guanine of the tetrads.

In order to expand the scope of this methodology, we synthesized an alternative new furan-equipped G4-ligand based on a different scaffold, featuring another well-established G4-binding motif (pyridine-2,6-dicarboxamides, PDC).[4b,12] The synthetic route was adapted to include a furan moiety, linked with a long spacing unit to the PDC core (**PDC-A**, Fig. 1). The insertion of a linker to outdistance the pro-reactive unit from the G4-binding core, and to maximize the interactions with the target, is in line with previous literature reports.[4b] Also here, the ligand oxidation rate in presence of G4-DNA is only marginally affected by MB dilution (Fig. S10, ESI†). In alkylation experiments, **PDC-A** showed a slightly lower conversion (up to 54.6%) with formation of a single peak in the HPLC-UV chromatogram

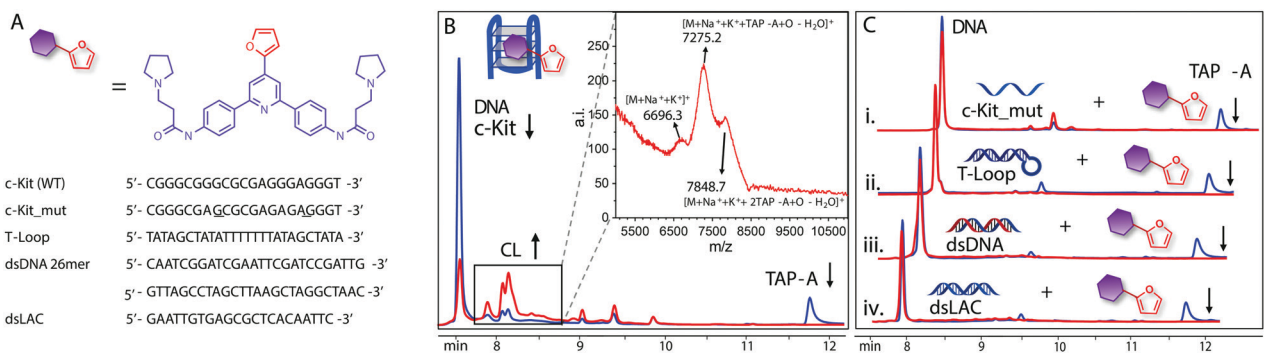

Fig. 3 HPLC-UV G4-alkylation experiments using **TAP-A** (25 μM) with the sequences depicted in panel (A) (5 μM), at 0 (blue) and 30 (red) minutes of irradiation, in Tris HCl buffer (pH 7.4, 10 mM K^+). (B) With c-Kit (WT), at 0.1 μM MB. The inset shows the corresponding MALDI-TOF spectrum. (C) Negative controls with ssDNA c-Kit_mut (i) and dsDNA sequences at 2 μM MB: T-Loop (ii), dsDNA 26mer (iii) and dsLAC (iv).

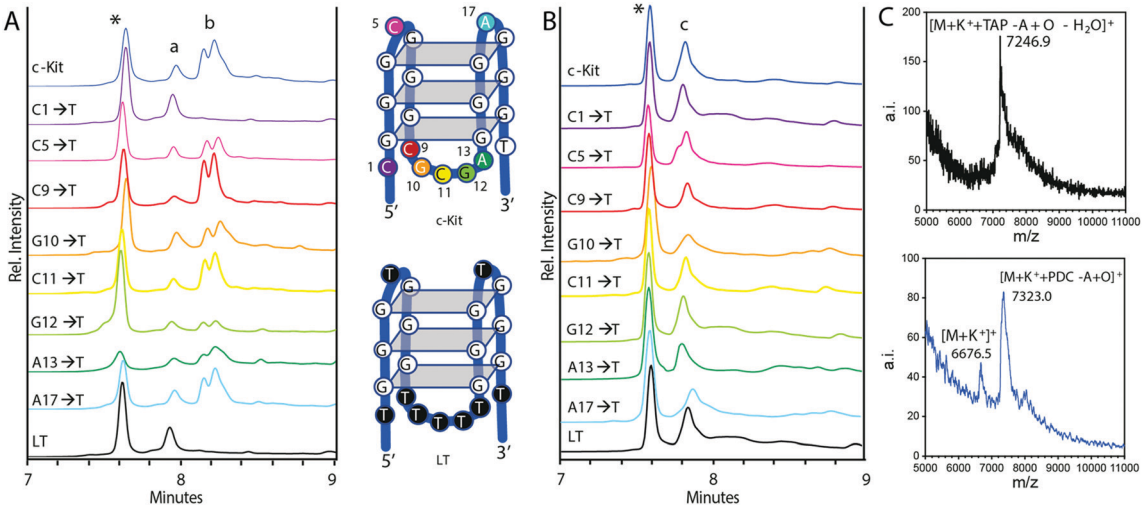

Fig. 4 Alkylation experiments of **TAP-A** (A) and **PDC-A** (B), 25 μM, in Tris HCl buffer (pH 7.4, 10 mM K^+), at 0.1 μM MB concentration. Each chromatogram indicates a substitution of loop nucleobases with a thymine. * = Residual DNA peak; a = **TAP-A** mono-alkylation peak; b = **TAP-A** di-alkylation peak; c = **PDC-A** alkylation peak. (C) MALDI-TOF spectra of the isolated adducts of **TAP-A** with c-Kit LT (top) and **PDC-A** with C-Kit WT (bottom).

(rt = 7.8 min, Fig. 4B) corresponding to the mono-alkylation product as confirmed by MALDI-TOF (+648 Da, Fig. 4C). In the thymine-substitution experiment, similar HPLC profiles were obtained in all cases (Fig. 4B). As these results suggest a direct alkylation of the tetrads, molecular docking studies were performed to identify the binding modes and the possible reacting nucleophiles. Using a validated protocol,[13a] ensemble docking was performed on 10 conformations of c-Kit available from NMR coordinates (PDB ID: 2KQH), to consider the flexibility of the target, including loop movements. Taking into account the energy scores (*i.e.* most stable binding modes, Fig. S23, ESI†), the top five docking solutions of **TAP-A** were encountered with c-Kit conformers #9 (ranked 1 to 4) and #7 (ranked 5). The four docking solutions obtained with the c-Kit conformer #9 depict a similar positioning of **TAP-A** (Fig. S24A, ESI†). The same protocol was followed with oxidized **TAP-A** on the c-Kit conformer #9, showing a preserved binding mode (Fig. S24B, ESI†). In this binding mode, we did not detect any NH_2 residue within a threshold distance of 4.0 Å from the **TAP-A** keto–enol reactive carbon. These docking solutions can thus not explain our results, illustrating a stable but 'non-reactive' binding mode. However, it is known that TAP-based ligands feature multiple binding modes with c-Kit.[13b] Hence, the fifth-top docking solution is an alternative binding mode obtained with c-Kit conformer #7 (Fig. S23, ESI†), also preserved with oxidized **TAP-A** (Fig. S24, ESI†). The pyrrolidinylpropanamide chain is docked in the single-nucleotide loop L3 formed by A17 (Fig. S24, ESI†), positioning the reactive carbonyl of the keto–enol chain at a distance of 3.7 Å from the G12 exocyclic amine (Fig. 5A). Although C1 is still distant (7.0 Å, Fig. 5A), the flexibility of the keto–enol makes the alkylation possible when extending our structural analysis to the top 3 docking solutions of oxidized **TAP-A** with c-Kit conformer #7 (Fig. S26, ESI†). The C1-distance decreases to 3.8 Å or 4.2 Å in the second and third docking solutions, respectively, whereas G12 distance is 4.2 Å and 5.1 Å in the same docking solutions. The results are in agreement with the thymine substitution experiments for **TAP-A**. For **PDC-A**, the five most stable docking poses are encountered with c-Kit conformer #8 (scores in Fig. S23 and poses in S27A, ESI†). As for **TAP-A**, oxidation of **PDC-A** does not influence the binding mode, the most stable docking solution of both furan-closed and oxidized forms of **PDC-A** being superimposed (Fig. S27B, ESI†). **PDC-A** is mainly docked in the lateral loop 'L2' ($C_9G_{10}C_{11}G_{12}A_{13}$), and it orients the reactive carbon close to several c-Kit exocyclic amines, *i.e.* C11 (3.8 Å), G8 (6.1 Å), and G10 (6.4 Å), a residue belonging to a central quartet (Fig. 5B). Considering the oxidized **PDC-A** docking solutions #2 and #3 of (Fig. S28, ESI†), the G8 distance decreases from 5.8 Å in the second docking solution (3.8 Å for C11) to 3.9 Å in the third-best ranked solution (Fig. S28, ESI†), whereas the C11 distance increases to 5.3 Å. It is important to underline that, although the keto–enol chain is located in a similar c-Kit region for the three-best ranked docking solutions of oxidized **PDC-A** with c-Kit conformer #8, quinolinium moieties are not well superimposed (Fig. S28, ESI†), highlighting a possible competition between two **PDC-A** binding sites following its oxidation that could explain why we do not observe reactivity with the C11 residue, but rather G8/G10. Altogether, these docking results provide the 'reactive' binding modes of the ligands as well as insights to understand the alkylation profile obtained in our experiments, giving clues on the possible residues involved in the alkylation. In addition, docking simulations confirm the possibility for simultaneous co-localization of MB and each ligand studied here on the same G4, with MB interacting with the lower G4 tetrad (see ESI,† Section 10 and Fig. S33).

These results were validated by synthesizing and testing additional furan-containing ligands (**TAP-B** and **PDC-B**), bearing a spacing unit to outdistance the furan from the supposed reactive residues, resulting in a reduced alkylation efficiency (please refer to Section 9 and 10 in ESI†). Finally, we have tested the furan-mediated alkylation to two other relevant G4-forming sequences, c-Myc and h-Telo (Table S2, ESI†). Preliminary results

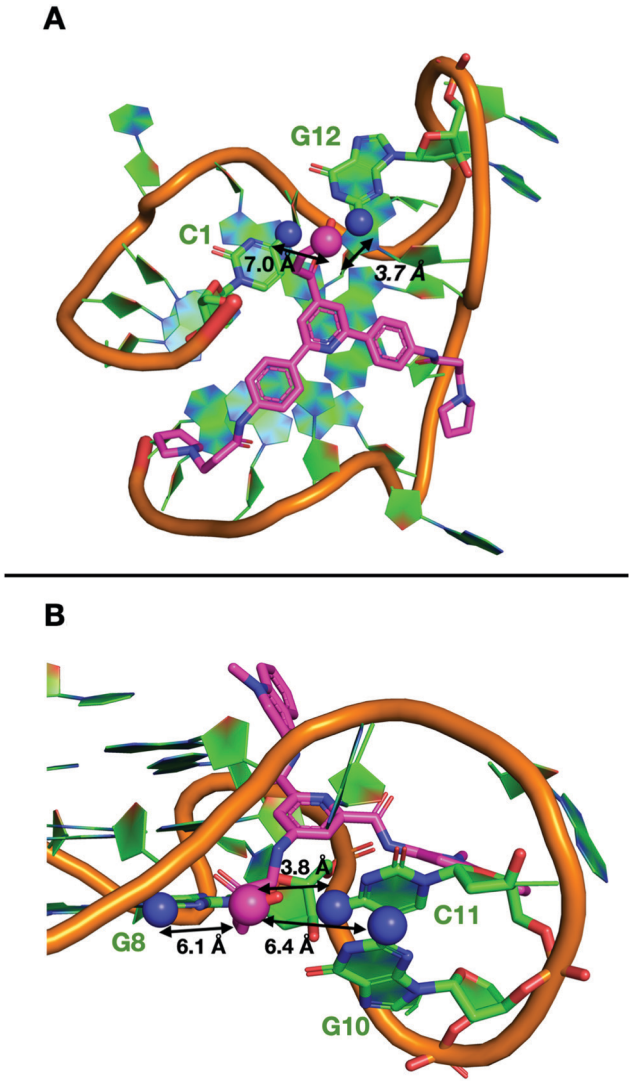

Fig. 5 Top ranked docking poses for the oxidized forms of **TAP-A** (A) and **PDC-A** (B) as obtained with the c-Kit conformers #7 and #8, respectively (PDB ID: 2KQH). The ligands are depicted in purple. The reactive carbon of each keto–enol chain is represented with a purple sphere. The nitrogen atoms of the closest exocyclic amines are depicted in blue spheres, and the corresponding nucleobases are shown with thick sticks and textually highlighted.

illustrate that **TAP-A** is able to alkylate h-Telo, while **PDC-A** showed a preferential alkylation for c-Myc (see Section 9 in ESI†).

In conclusion, we illustrated an alternative and efficient methodology to selectively target G4-DNA, applicable to existing (**TAP-A**) or newly designed (**PDC-A**) G4 ligands. The small steric requirements and the chemical robustness of the furan moiety render its use advantageous as compared to other alkylating moieties,[3] making its incorporation into ligands easier, without undermining the ligands' ability to bind G4-DNA. The use of G4-binding photosensitizers allows the local pinpoint production of the required $^1O_2$, avoiding collateral oxidative damage. MB was selected because of its availability and the established use in therapeutic contexts,[14] but the methodology can be further extended to other G4-ligands with photosensitizing ability, such as cationic porphyrins, already used in the context of photodynamic therapy to localize $^1O_2$ production close to G4-RNA sequences.[15] Given the large number of existing G4-ligand types, we envisage the expansion of this methodology to other classes of compounds, with the aim of targeting different G4-forming sequences of various topologies.

This work was supported by the FWO and the European Union's Horizon 2020 research and innovation programme under the Marie Skłodowska-Curie grant agreement no. 665501 (Al. M.) and 721613 (EC). Research in Mons was supported by Excellence of Science (F.R.S.-FNRS/FWO) under the Grant No. 30650939 (PRECISION). Computational resources have been provided by the Consortium des Équipements de Calcul Intensif (CÉCI), under F.R.S.-FNRS Grant No. 2.5020.11.

Conflicts of interest

There are no conflicts to declare.

References

1 (*a*) A. Siddiqui-Jain, C. L. Grand, D. J. Bearss and L. H. Hurley, *Proc. Natl. Acad. Sci. U. S. A.*, 2002, **99**, 11593–11598; (*b*) A. T. Phan, V. Kuryavyi, S. Burge, S. Neidle and D. J. Patel, *J. Am. Chem. Soc.*, 2007, **129**, 4386–4392; (*c*) Y. Xu, K. Kaminaga and M. Komiyama, *J. Am. Chem. Soc.*, 2008, **130**, 11179–11184; (*d*) K. W. Lim, S. Amrane, S. Bouaziz, W. Xu, Y. Mu, D. J. Patel, K. N. Luu and A. T. Phan, *J. Am. Chem. Soc.*, 2009, **131**, 4301–4309.
2 (*a*) G. Biffi, D. Tannahill, J. McCafferty and S. Balasubramanian, *Nat. Chem.*, 2013, **5**, 182–186; (*b*) S. Neidle, *J. Med. Chem.*, 2016, **59**, 5987–6011; (*c*) A. R. Duarte, E. Cadoni, A. S. Ressurreição, R. Moreira and A. Paulo, *ChemMedChem*, 2018, **13**, 869–893; (*d*) D. Varshney, J. Spiegel, K. Zyner, D. Tannahill and S. Balasubramanian, *Nat. Rev. Mol. Cell Biol.*, 2020, **21**, 459–474.
3 M. P. O'Hagan, J. C. Morales and M. C. Galan, *Eur. J. Org. Chem.*, 2019, 4995–5017.
4 (*a*) M. Nadai, F. Doria, L. Germani, S. N. Richter and M. Freccero, *Chem. – Eur. J.*, 2015, **21**, 2330–2334; (*b*) D. Verga, F. Hamon, F. Poyer, S. Bombard and M. P. Teulade-Fichou, *Angew. Chem., Int. Ed.*, 2014, **53**, 994–998; (*c*) E. Morel, F. Poyer, L. Vaslin, S. Bombard and M. P. Teulade-Fichou, *Inorg. Chim. Acta*, 2016, **452**, 152–158.
5 (*a*) M. O. De Beeck and A. Madder, *J. Am. Chem. Soc.*, 2011, **133**, 796–807; (*b*) A. Manicardi, E. Gyssels, R. Corradini and A. Madder, *Chem. Commun.*, 2016, **52**, 6930–6933.
6 (*a*) M. Op De Beeck and A. Madder, *J. Am. Chem. Soc.*, 2012, **134**, 10737–10740; (*b*) N. De Laet, E. M. Llamas and A. Madder, *ChemPhotoChem*, 2018, **2**, 575–579.
7 N. M. Smith, G. Labrunie, B. Corry, P. L. T. Tran, M. Norret, M. Djavaheri-Mergny, C. L. Raston and J. L. Mergny, *Org. Biomol. Chem.*, 2011, **9**, 6154–6162.
8 F. T. Zhang, J. Nie, D. W. Zhang, J. T. Chen, Y. L. Zhou and X. X. Zhang, *Anal. Chem.*, 2014, **86**, 9489–9495.
9 D. van Straten, V. Mashayekhi, H. S. de Bruijn, S. Oliveira and D. J. Robinson, *Cancers*, 2017, **9**, 1–54.
10 R. W. Redmond and J. N. Gamlin, *Photochem. Photobiol.*, 1999, **70**, 391–475.
11 K. Stevens and A. Madder, *Nucleic Acids Res.*, 2009, **37**, 1555–1565.
12 A. Renaud De La Faverie, F. Hamon, C. Di Primo, E. Largy, E. Dausse, L. Delaurire, C. Landras-Guetta, J. J. Toulmé, M. P. Teulade-Fichou and J. L. Mergny, *Biochimie*, 2011, **93**, 1357–1367.
13 (*a*) C. Kotras, M. Fossépré, M. Roger, V. Gervais, S. Richeter, P. Gerbier, S. Ulrich, M. Surin and S. Clément, *Front. Chem.*, 2019, **7**, 493; (*b*) A. Kerkour, J.-L. Mergny and G. F. Salgado, *Biochim. Biophys. Acta, Gen. Subj.*, 2017, **1861**, 1293–1302.
14 P. R. Ginimuge and S. D. Jyothi, *J. Anaesthesiol., Clin. Pharmacol.*, 2010, **26**, 517–520.
15 A. Ferino, G. Nicoletto, F. D'Este, S. Zorzet, S. Lago, S. N. Richter, A. Tikhomirov, A. Shchekotikhin and L. E. Xodo, *J. Med. Chem.*, 2020, **63**, 1245–1260.